

On the universality class of the 3d Ising model with long-range-correlated disorder

D. Ivaneyko ^{a,*}, B. Berche ^b, Yu. Holovatch ^{c,d}, J. Ilnytskyi ^{c,e}

^a*Ivan Franko National University of Lviv, 79005 Lviv, Ukraine*

^b*Laboratoire de Physique des Matériaux, Université Henri Poincaré, Nancy 1, 54506 Vandœuvre les Nancy Cedex, France*

^c*Institute for Condensed Matter Physics, National Acad. Sci. of Ukraine, 79011 Lviv, Ukraine*

^d*Institut für Theoretische Physik, Johannes Kepler Universität Linz, 4040 Linz, Austria*

^e*Institut für Physik, Universität Potsdam, 14469 Potsdam, Deutschland*

Abstract

We analyze a controversial topic about the universality class of the three-dimensional Ising model with long-range-correlated disorder. Whereas both theoretical and numerical studies agree on the validity of extended Harris criterion (A. Weinrib, B.I. Halperin, Phys. Rev. B 27 (1983) 413) and indicate the existence of a new universality class, the numerical values of the critical exponents found so far differ essentially. To resolve this discrepancy we perform extensive Monte Carlo simulations of a 3d Ising model with non-magnetic impurities being arranged in a form of lines along randomly chosen axes of a lattice. The Swendsen-Wang algorithm is used alongside with a histogram reweighting technique and the finite-size scaling analysis to evaluate the values of critical exponents governing the magnetic phase transition. Our estimates for these exponents differ from both previous numerical simulations and are in favour of a non-trivial dependency of the critical exponents on the peculiarities of long-range correlations decay.

Key words: random Ising model, long-range-correlated disorder, Monte Carlo, critical exponents

PACS: 05.10.Ln, 64.60.Fr, 75.10.Hk

* Corresponding author.

Email addresses: ivaneiko@kthfranko.lviv.ua (D. Ivaneyko), berche@lpm.u-nancy.fr (B. Berche), hol@icmp.lviv.ua (Yu. Holovatch), iln@icmp.lviv.ua (J. Ilnytskyi).

1 Introduction

Critical properties of structurally disordered magnets remain a problem of great interest in condensed matter physics, as far as real magnetic crystals are usually non-ideal. Commonly, in the theoretical studies, as well as in the MC simulations, one considers point-like uncorrelated quenched non-magnetic impurities [1]. However, in real magnets one encounters non-idealities of structure, which cannot be modeled by simple point-like uncorrelated defects. Indeed, magnetic crystals often contain defects of a more complex structure: linear dislocations, planar grain boundaries, three-dimensional cavities or regions of different phases, embedded in the matrix of the original crystal, as well as various complexes (clusters) of point-like non-magnetic impurities [2]. Therefore, a challenge is to offer a consistent description of the critical phenomena influenced by the presence of such complicated defects.

Different models of structural disorder have arisen as an attempt to describe such defects. In this paper we concentrate on the so-called long-range-correlated disorder when the point-like defects are correlated and the resulting critical behaviour depends on the type of this correlation. Several models have been proposed for description of such a dependence [3–6], a subject of extensive analytical [4–14] and numerical [6, 14–17] treatment. A common outcome of the above studies is that although the concentration of non-magnetic impurities is taken to be far from the percolation threshold, in the region of weak dilution, the impurities make a crucial influence on an onset of ordered ferromagnetic phase. Given that the pure (undiluted) magnet possesses a second-order phase transition at certain critical temperature T_c , an influence of the weak dilution may range from the decrease of T_c to the changes in the universality class and even to the smearing off this transition [14]. Moreover, the critical exponents governing power law scaling in the vicinity of T_c may depend on the parameters of impurity-impurity correlation.

To give an example, the Harris criterion, which holds for the energy-coupled uncorrelated disorder [18] is modified when the disorder is long-range correlated [5, 7]. In particular, when the impurity-impurity pair correlation function $g(r)$ decays at large distances r according to a power law:

$$g(r) \sim 1/r^a, \quad r \rightarrow \infty \quad (1)$$

the asymptotic critical exponents governing magnetic phase transition (and hence the universality class of the transition) do change if [5]

$$\nu^{\text{pure}} < 2/a, \quad (2)$$

where ν^{pure} is the correlation length critical exponent of the undiluted magnet.

The above condition (2) holds for $a < d$, d being the space (lattice) dimension. For $a > d$ the usual Harris criterion [18] is recovered and condition (2) is substituted by $\nu^{\text{pure}} < 2/d$.

The fact, that the power of the correlation decay might be a relevant parameter at $a < d$ can be easily understood observing an asymptotics of the Fourier transform g_k of $g(r)$ at small wave vector numbers k . From (1) one arrives at $g_k \sim k^{a-d}$, which for $a < d$ leads to a singular behaviour at $k \rightarrow 0$. As far as the small k region defines the criticality, the systems with $a < d$ are good candidates to manifest changes in the critical behaviour with respect to their undiluted counterparts. On contrary, impurity-impurity correlations at $a > d$ do not produce additional singularities with respect to the uncorrelated point-like impurities, therefore they are referred to as the short-range correlated. In turn, the disorder characterized by Eq. (1) with $a < d$ is called the long-range correlated.

There are different ways to model systems with the long-range-correlated disorder governed by Eq. (1). The most direct interpretation relies on the observation that the integer a in Eq. (1) corresponds to the large r behaviour of the pair correlation function for the impurities in the form of points ($a = d$), lines ($a = d - 1$), and planes ($a = d - 2$) [5]. Since the last two objects extend in space, the impurities with $a < d$ sometimes are called the extended ones. Note that the isotropic form of the pair correlation function (1) demands random orientation of such spatially extended objects.¹ Non-integer a sometimes are treated in terms of a fractal dimension of impurities, see e.g. [19]. Besides energy-coupled disorder, the power-law correlation decay (1) is relevant for the thermodynamic phase transition in random field systems [20], percolation [21], scaling of polymer macromolecules at presence of porous medium [22,23], zero-temperature quantum phase transitions [24].

Our paper was stimulated by the observations of obvious discrepancies in the state-of-the-art analysis of criticality in three-dimensional Ising magnets with the long-range-correlated disorder governed by Eq. (1). Indeed, since for the pure $d = 3$ Ising model $\nu^{\text{pure}} = 0.6304(13)$ [25], the long-range correlated disorder should change its universality class according to Eq. (2). Whereas both theoretical and numerical studies agree on the validity of extended Harris criterion (2) and bring about the new universality class [5, 12, 15, 16], the numerical values of the critical exponents being evaluated differ essentially. We list the values of the exponents found so far by different approaches in table 1 and refer the reader to the section 2 for a more detailed discussion of this issue. Here, we would like to point out that presently the results of each of existing analytical approaches (Refs. [5] and [12]) is confirmed by only one

¹ Anisotropic distributions of extended impurities are treated in Refs. [3, 4, 7–9, 11, 14].

numerical simulation (Refs. [15] and [16], respectively). To resolve such a bias, we perform MC simulations of a $d = 3$ Ising model with extended impurities and evaluate critical exponents governing ferromagnetic phase transition. As it will become evident from the further account, our estimates for the exponents differ from the results of two numerical simulations performed so far [15, 16] and are in favour of a non-trivial dependency of the critical exponents on the peculiarities of long-range correlations decay.

Reference	ν	γ	β	η
Weinrib, Halperin, [5]	1	2	1/2	0
Prudnikov <i>et al.</i> , [12]	0.7151	<i>1.4449</i>	<i>0.3502</i>	-0.0205
Ballesteros, Parisi, [15] ^a	1.012(10)	<i>1.980(16)</i>	<i>0.528(7)</i>	0.043(4)
[15] ^b	1.005(14)	<i>1.967(23)</i>	<i>0.524(9)</i>	0.043(4)
Prudnikov <i>et al.</i> , [16] ^a	0.719(22)	<i>1.407(24)</i>	0.375(45)	<i>0.043(93)</i>
[16] ^b	0.710(10)	1.441(15)	0.362(20)	<i>-0.030(7)</i>

Table 1

The critical exponents for the three-dimensional Ising model with extended impurities for $a = 2$. Renormalization group calculations: first order ε, δ -expansion [5]; two-loop massive renormalization scheme [12]. Monte Carlo simulations: finite-size scaling, combination of Wolff and Swendsen-Wang algorithms, magnetic site concentration $p = 0.8$ [15]^a, $p = 0.65$ [15]^b; short-time critical dynamics with Metropolis algorithm, $p = 0.8$ [16]^a, finite-size scaling with Wolff algorithm, $p = 0.8$ [16]^b. Values of the exponents obtained from the scaling relations are shown in italic (see section 2 for a more detailed discussion).

The outline of the paper is the following. In the next section we make a brief overview of the results of previous analysis of the 3d Ising model with long-range-correlated impurities paying special attention to the former MC simulations. Details of our MC simulations are explained in sections 3 and 4. There, we formulate the model and define the observables we are interested in. We analyze statistics of typical and rare events taking the magnetic susceptibility as an example in section 4. The numerical values of the exponents are evaluated there by the finite-size scaling technique. Section 5 concludes our study.

2 Overview of previous analytical and MC results

Currently, there exist two different analytical results for the values of critical exponents of the 3d Ising model with long-range-correlated impurities. The

first one is due to Weinrib and Halperin, who formulated the model of a m -vector magnet with quenched impurities correlated via the power law (1) [5]. They used the renormalization group technique carrying out a double expansion in $\varepsilon = 4 - d$, $\delta = 4 - a$, considering ε and δ to be of the same order of magnitude, and estimating values of the critical exponents to the first order in this expansion. Further, they conjectured the obtained first order result for the correlation length critical exponent

$$\nu = 2/a \tag{3}$$

to be an exact one and to hold for any value of spin component number m provided that $\nu^{\text{pure}} < 2/a$. By complementing Eq. (3) with the first order value of the pair correlation function critical exponent, $\eta = 0$ [5], the other critical exponents can be obtained via familiar scaling relations. For $a = 2$ the exponents are listed in table 1.

The second theoretical estimate was obtained by Prudnikov *et al.* [12] in the field theoretical renormalization group technique by performing renormalization for non-zero mass at fixed space dimension $d = 3$. Their two-loop calculations refined by the resummation of the series obtained bring about a non-trivial dependence of the critical exponents both on m and on a . We list their values of the exponents for $m = 1$ and $a = 2$ in the second row of table 1. In particular, one observes that the correlation length exponent ν obtained in Ref. [12] differs from the value predicted by (3) by the order of 25 %. As for the reason of such discrepancy the authors of Ref. [12] point to a higher order of the perturbation theory they considered together with the methods of series summation as well as to taking into account the graphs which are discarded when the ε, δ -expansion is being used.

Let us note however, the qualitative agreement between the above analytical results: both renormalization group treatments, Refs. [5] and [12], predict that the new (long-range-correlated) fixed point is stable and reachable for the condition considered and hence the 3d Ising model with long-range-correlated impurities belongs to a new universality class. These are only the numerical values of the exponents which call for additional verification. In such cases one often appeals to the numerical simulations. Indeed, two simulations were performed, and, strangely enough, the results again split into two groups: whereas the simulation of Ballesteros and Parisi [15] is strongly in favour of the theoretical results of Weinrib and Halperin, the simulation of Prudnikov *et al.* [16] almost exactly reproduces former theoretical results of this group [12] as one can see from table 1. There, we give the results for the exponents obtained in simulations complementing them by those that follow if one uses familiar scaling relations (the last are shown in italic).

Since our own study will rely on the simulation technique as well, we describe an analysis performed in Refs. [15, 16] in more details. In Ref. [15] the simulations were done for two different types of the long-range-correlated disorder referred by the authors as the Gaussian and the non-Gaussian one. In the first case, the point-like defects are scattered directly on the sites of a 3d simple cubic lattice according to the desired decay of the pair correlation function (1), $a = 2$. In the second case, the defects form the lines directed along the randomly chosen axes and, as was mentioned before, their impurity-impurity pair correlation function should also decay at large r as $g(r) \sim 1/r^2$. The MC algorithm used in Ref. [15] is a combination of a single-cluster Wolff method and a Swendsen-Wang algorithm. After a fixed number of a single-cluster updates one Swendsen-Wang sweep is performed. The procedure was called a MC step (MCS). The number of single cluster flips was chosen such that the autocorrelation time τ_E was typically 1 MCS. For thermalization of the system 100 MCSs were performed and then various observables were measured. The simulation was done on the lattice of sizes $L = 8, 16, 32, 64$ and 128. Then 100 MCSs have been used for measurements on $N_S=20000$ different samples for $L \leq 64$ and on $N_S=10000$ samples for $L = 128$. The procedure seems to be quite safe.

Values of the critical exponents ν and η obtained in Ref. [15] in the case of Gaussian disorder (point-like long-range-correlated defects) are given in table 1 for the impurities concentrations $p = 0.8, p = 0.65$. It was stated in the paper, that for the non-Gaussian disorder (lines of defects) the estimates of the exponents are comparable with analytic calculations of Weinrib and Halperin [5].

In Ref. [16] the MC simulation of the critical behavior of the three-dimensional Ising model with long-range-correlated disorder at criticality was performed by means of the short-time dynamics and the single-cluster Wolff method. Randomly distributed defects had a form of lines and resembled the "non-Gaussian disorder" of Ref. [15]. However, in contrast to Ref. [15], a condition of lines mutual avoidance was implemented. According to Ref. [16], a situation when crossing of the lines of defects is allowed is not described by the Weinrib-Halperin model. In the short-time critical dynamics method, the concentration of spins was chosen $p = 0.8$ and the cubic lattices of sizes $L = 16 \div 128$ were considered. As a MC method was used a Metropolis algorithm. Resulting numbers for the exponents are given in the 5th row of table 1.

Additional simulations in the equilibrium state were performed in Ref. [16] to verify the reliability of results obtained by means of the short-time critical dynamics. The single-cluster Wolff algorithm was used for simulation and a finite size scaling for evaluation of the critical exponents. One MCS was defined as 5 cluster flips, 10^4 MCSs were discarded for equilibration and 10^5 for measurement. Disorder averaging was typically performed over 10^4 samples. Again,

the procedure seems to be safe. The values of critical exponents obtained in the simulations are quoted in the 6th row of table 1.

With the above information at hand we started our numerical analysis as explained in the forthcoming sections.

3 Model and observables

We consider a $d = 3$ Ising model with non-magnetic sites arranged in a form of randomly oriented lines (see Fig. 1). The Hamiltonian reads:

$$\mathcal{H} = -J \sum_{\langle ij \rangle} c_i c_j S_i S_j, \quad (4)$$

where $\langle ij \rangle$ means the nearest neighbour summation over the sites of a s.c. lattice of linear size L , $J > 0$ is the interaction constant, Ising spins $S_i = \pm 1$, $c_i = 0; 1$ is the occupation number for the i -th site and periodic boundary conditions are employed. Non-magnetic sites ($c_i = 0$) are quenched in a fixed configuration and form lines, as shown in Fig. 1. Concentration p of the magnetic sites is taken to be far above the percolation threshold. Fig. 1 shows one possible configuration for non-magnetic impurity lines. During the simulations, one generates a large number of such disorder realizations. This is done in our study using the following procedure. The lines of impurities are generated one by one, each along randomly chosen axis and the final disorder realization is accepted with the probability

$$P(p) = \exp(-(p - p_{\text{req}})^2 / \sigma^2) \quad (5)$$

using rejection method. Here p_{req} is a required value for the concentration of magnetic sites and σ is the dispersion of the resulted Gaussian distribution in p (see Fig. 11). The average value for the impurity concentration is equal to $1 - p$. In the simulations presented here we paid special attention to the width of this distribution and consider both broad and narrow cases, see sections 4.2 and 4.3).

The observables saved during each step of the MC simulations for a given disorder realization will be the instantaneous values for the internal energy \mathcal{E} and magnetisation \mathcal{M} per spin, defined as

$$\mathcal{E} = -J \frac{1}{N_p} \sum_{\langle ij \rangle} c_i c_j S_i S_j, \quad (6)$$

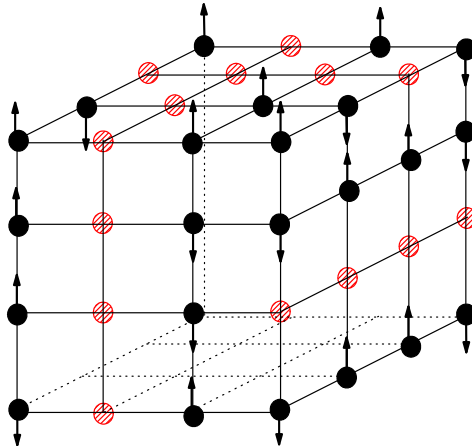


Figure 1. A 3d Ising model with long-range-correlated disorder in the form of randomly oriented lines of non-magnetic sites. Magnetic sites are shown by discs with arrows, non-magnetic sites are dashed (red on-line) and do not hold arrows.

$$\mathcal{M} = \frac{1}{N_p} \sum_i c_i S_i, \quad (7)$$

where number of magnetic sites is $N_p = pN$, total number of sites is $N = L^3$. Using the histogram reweighting technique [26] we compute the following expectation values at the critical temperature region for a given disorder realization:

$$\langle \mathcal{E} \rangle, \quad \langle |\mathcal{M}| \rangle, \quad \langle \mathcal{M}^2 \rangle, \quad \langle \mathcal{M}^4 \rangle \quad (8)$$

as functions of an inverse temperature $\beta = 1/T$. In (8) the angular brackets $\langle \dots \rangle$ stand for the thermodynamical averaging in one sample of disorder.

For a given disorder configuration, one can evaluate the temperature behaviour of the magnetic susceptibility χ and magnetic cumulants U_2, U_4 :

$$\chi = \beta J N_p (\langle \mathcal{M}^2 \rangle - \langle |\mathcal{M}| \rangle^2), \quad U_4 = 1 - \frac{\langle \mathcal{M}^4 \rangle}{3 \langle \mathcal{M}^2 \rangle^2}, \quad U_2 = 1 - \frac{\langle \mathcal{M}^2 \rangle}{3 \langle |\mathcal{M}| \rangle^2}. \quad (9)$$

In order to refer to the physical quantities, the observables are to be averaged over different disorder configurations, denoted hereafter by an overline: $\overline{(\dots)}$. Two ways of averaging can be found in the literature, which we will consider for the case of finding the maximum value for the susceptibility. At each disorder realization an individual curve for the susceptibility χ as a function of the temperature T is obtained (using histogram reweighting technique). In the first method of averaging, depicted in Fig. 2,a the maximal values of each individual curves are averaged over all disorder realizations. This type

of averaging, referred hereafter as *averaging a*, will be denoted as $\overline{\chi_{\max}}$. An

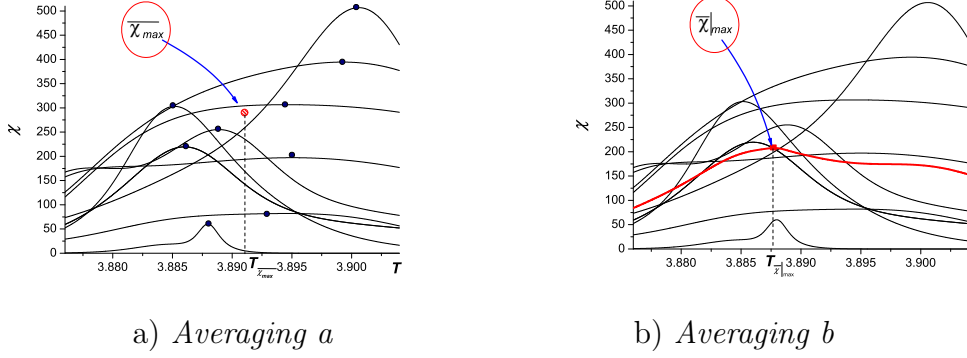


Figure 2. Two ways to perform an averaging over disorder configurations. *Averaging a*: the maximal values of magnetic susceptibility are found for each disorder realization (black discs) and averaged over disorder configurations. The resulting averaged value $\overline{\chi_{\max}}$ is shown by the red square. *Averaging b*: the configurational averaging of χ is performed (red dashed curve) and a maximum of the resulting curve $\overline{\chi}|_{\max}$ is found (red square).

alternative method is shown in Fig. 2, b: at first one performs a configurational averaging of the susceptibility, i.e. the single averaged curve is evaluated for $\overline{\chi(T)}$. Then the maximal value for this curve, $\overline{\chi}|_{\max}$, is found. Hereafter, this method will be referred as *averaging b*. Both *averaging a* and *averaging b* will be exploited in our analysis.

To evaluate the critical exponents, a number of characteristics will be used with known finite size scaling:

- *averaging a*:

$$\overline{\chi_{\max}}, \quad \overline{\langle |\mathcal{M}| \rangle}_{\max}, \quad D_{U_4} = \left. \frac{\partial U_4}{\partial \beta} \right|_{\max}, \quad D_{U_2} = \left. \frac{\partial U_2}{\partial \beta} \right|_{\max}. \quad (10)$$

Here, $\overline{\chi_{\max}}$, D_{U_4} , and D_{U_2} are the averaged over disorder configurations maximal values of the magnetic susceptibility and magnetic cumulants temperature derivatives. The value $\overline{\langle |\mathcal{M}| \rangle}_{\max}$ is calculated for the temperature that corresponds to the magnetic susceptibility maximum.

- *averaging b*:

$$\overline{\chi}|_{\max}, \quad \overline{\langle |\mathcal{M}| \rangle}|_{\max}, \quad \mathcal{D}_{U_4} = \left. \frac{\partial \mathcal{U}_4}{\partial \beta} \right|_{\max}, \quad \mathcal{D}_{U_2} = \left. \frac{\partial \mathcal{U}_2}{\partial \beta} \right|_{\max}, \quad (11)$$

$$\mathcal{D}_M = \left. \frac{\partial \log \overline{\langle |\mathcal{M}| \rangle}}{\partial \beta} \right|_{\max}, \quad \mathcal{D}_{M^2} = \left. \frac{\partial \log \overline{\langle \mathcal{M}^2 \rangle}}{\partial \beta} \right|_{\max}, \quad (12)$$

where

$$\mathcal{U}_4 = 1 - \frac{\overline{\langle \mathcal{M}^4 \rangle}}{3\overline{\langle \mathcal{M}^2 \rangle}^2}, \quad \mathcal{U}_2 = 1 - \frac{\overline{\langle \mathcal{M}^2 \rangle}}{3\overline{\langle |\mathcal{M}| \rangle}^2}. \quad (13)$$

Note, that quantities (12) are ill-defined if *averaging a* is considered. Moreover, as one can see from the definitions (9), (13) there are different ways to define magnetic cumulants for the disordered system (see Refs. [27] for more discussion).

We performed our numerical simulations using the Swendsen-Wang cluster algorithm. The main reason is, that with the diluted system one often performs simulations at the temperature which is far from the native phase transition point of each particular disorder realization. As the result, the single clusters can be of rather small size and the Wolff one algorithm, used by us before [33] is found to be less effective. The following set of lattice sizes $L = 6 \div 96$ ($L = 6 \div 128$ in some cases) is used and performing the finite-size-scaling analysis is performed. The magnetic site concentration is chosen to be $p = 0.8$ which is far from the percolation threshold and this also allows comparison with the previous simulations [15, 16]. Another reason for such a choice is that for the 3d Ising model with uncorrelated impurities the correction to scaling terms were found to be minimal at $p = 0.8$ [1, 28], (obviously, this does not mean that $p = 0.8$ minimizes correction-to-scaling terms at any level of impurities correlation). The number of samples ranges from 10^3 to 10^4 for all lattice sizes. The simulations are performed at the finite-size critical temperature $T_c(L)$ which is found from the maximum of magnetic susceptibility χ at each lattice size L and the reweighting technique for the neighbouring temperatures is used. Note, that in Refs. [15, 16] all simulation were performed at the critical temperature of an infinite system.

Similarly to our other previous papers [29, 30] we start simulation from estimating the critical temperature of a finite-size system as a function of the lattice size L , $T_c(L)$. For the smallest lattice size $L = 6$, the preliminary simulation is performed at pT_c^{pure} first (T_c^{pure} is the critical temperature for the pure system). The $T_c(L = 6)$ is located then from the maximum of the susceptibility. At the same time, we estimate various autocorrelation times to control the error due to time correlations. For the next larger lattice size, e.g. $L = 8$, preliminary simulation is performed at $T_c(L = 6)$ and then $T_c(L = 8)$ is located again from the maximum of the susceptibility at $L = 8$. The process is repeated for all lattice sizes. In this way we estimate $T_c(L)$ and the energy autocorrelation time $\tau_{\mathcal{E}}$. The results are given in table 2. One can see that the finite size system critical temperature obtained via *averaging a* differs from those obtained via and *averaging b*. The difference is not too large, the next simulations were performed at the critical temperature obtained by *averaging a*.

L	$\tau_{\langle \mathcal{E} \rangle}$	$T_c(L)$	
		$\overline{\chi_{\max}}$	$\overline{\chi} _{\max}$
6	2.50051	3.796779	3.795500
8	3.10875	3.812864	3.810200
10	3.39280	3.821152	3.817200
12	3.58191	3.829904	3.823000
16	3.90468	3.849101	3.842400
20	4.10689	3.855457	3.849200
26	4.28566	3.863750	3.860100
35	4.38278	3.871662	3.869700
48	4.4438	3.876678	3.874100
64	4.46380	3.881388	3.876900
96	4.26933	3.884435	3.881200
128	4.21278	3.886679	3.883220
		3.89124 ± 0.00057	3.89214 ± 0.00190
		3.89108 ± 0.00137	3.89033 ± 0.00139

Table 2

The critical temperature $T_c(L)$ of finite size system, obtained from maximum of magnetic susceptibility and autocorrelation times of absolute value of $\langle \mathcal{E} \rangle$ in the Swendsen-Wang cluster sweep.

In evaluation of the critical indices we followed the standard finite-size-scaling scheme as described e. g. in Ref. [26]. The estimates for the correlation length, magnetic susceptibility, and spontaneous magnetization critical exponents ν , γ and β can be obtained from the FSS behaviour of the following quantities:

- *averaging a:*

$$D_{U_4}, D_{U_2} \sim L^{1/\nu}, \quad \overline{\chi_{\max}} \sim L^{\gamma/\nu}, \quad \overline{\langle |\mathcal{M}| \rangle}_{\max} \sim L^{-\beta/\nu}, \quad (14)$$

- *averaging b:*

$$\mathcal{D}_{U_4}, \mathcal{D}_{U_2}, \mathcal{D}_M, \mathcal{D}_{M^2} \sim L^{1/\nu}, \quad \overline{\chi}|_{\max} \sim L^{\gamma/\nu}, \quad \overline{\langle |\mathcal{M}| \rangle}|_{\max} \sim L^{-\beta/\nu}. \quad (15)$$

In Eqs. (14), (15), the correction-to-scaling terms have been omitted. Taking them into account the FSS behaviour of the quantity A attains the form:

$$A \sim L^\phi (1 + \Gamma_A L^{-\omega}), \quad (16)$$

where ϕ is the leading exponent, ω is the correction-to-scaling exponent, and Γ_A is a correction-to-scaling amplitude. Hereafter, we perform the finite-size-scaling analysis in several ways. First, assuming the correction-to-scaling terms to be small we will fit the data for the observables to the leading power laws (14), (15) only. Besides that, we will also perform the fits with correction-to-scaling terms (16) as explained below.

4 Statistics of the observables. Preliminary estimates of the critical exponents

In this section, applying the above described formalism, we give preliminary estimates of the critical exponents. As we will see, the estimates for the same exponent obtained on the base of FSS of different quantities differ from each other. Moreover, similar differences arise when the results obtained via *averaging a* and *averaging b* are compared. We will discuss possible reasons for such behaviour and will analyze them further in the forthcoming section.

The starting point of the analysis performed in this section is connected with the fact that at the same concentration of impurities, different samples vary configurationally (geometrically) as well as in their thermodynamical characteristics. In systems with uncorrelated dilution these variations are also present (see e.g. Ref. [31]) although, as we will see below, these are less pronounced than in the case of the long-range-correlated disorder. Moreover, although the mean concentration of magnetic sites is well-defined for an ensemble samples (and chosen to be $p = 0.8$), the concentration of magnetic sites in each sample vary from the mean one. Such deviations are caused by possible intersections of impurity lines in different samples, besides not for all lattice sizes one can reach given concentration of impurities by an integer number of lines. Therefore, to start an analysis one has to make a choice of a set of sample specifying allowed values of the concentration dispersion. We start an analysis by dealing with the set of samples that are characterized by dispersion of concentrations $\sigma^2 = 10^{-4}$.

4.1 Typical, average, and rare values

The sample-to-sample variations increase with the increase of the lattice size. As an example, we show in Fig. 3 the values of the susceptibility for a given disorder realization calculated via *averaging a* ($\overline{\chi_{\max}}$, Fig. 3a-3c) and *averaging b* ($\overline{\chi}_{\max}$, Fig. 3d-3f) for three typical lattice sizes $L = 10, 26, 96$. Each point in these plots represents the data obtained for a given sample (i.e. given disorder realization). Solid lines are made up of the average values, where at each $\#$

the averaging is done on the interval $0 - \#$. One can see that the averages saturate at $\#$ larger than two hundred samples. From this in particular one can conclude that considered here number of samples $N_{dis} = 1000$ is quite sufficient for further analysis.

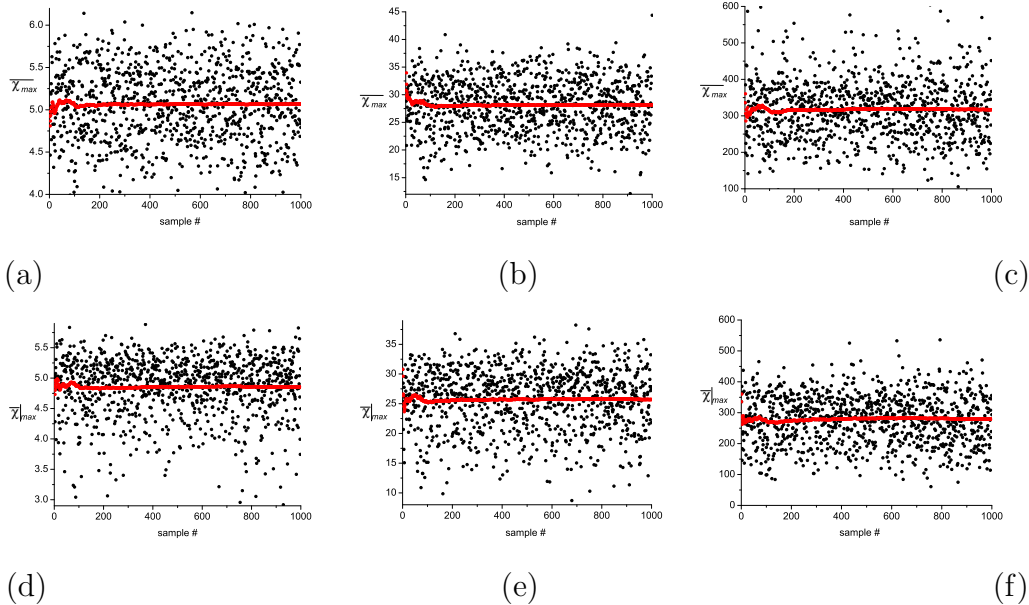


Figure 3. Values of the susceptibility $\overline{\chi_{\max}}$, calculated via *averaging a* (Fig. 3a-3c) and $\overline{\chi}_{\max}$, calculated via *averaging b* (Fig. 3d-3f) for different disorder realizations (different samples). Running average over the samples is shown by the solid line. From left to right: $L = 10, 26, 96$.

One observes that for some samples $\overline{\chi_{\max}}$ and $\overline{\chi}_{\max}$ differ significantly from the average values. When this is the case, we will call such an event a rare one. The values that are close to the maximal one will be referred to as typical events. We would like to stress that for *averaging b* for the lattice size $L = 10$ most of rare events produce the values for the susceptibility below the average value, while for $L = 96$ the situation is reversed, see figure 3. At $L = 26$ the distribution of rare events is approximately symmetric. The situation is more homogenous for the *averaging a*.

The averaging over too small number of disorder realizations leads to typical (i.e. most probable) values instead of averaged ones. Indeed, as can be seen in Fig. 4 for $L = 96$, the probability distributions of $\overline{\chi_{\max}}$ and $\overline{\chi}_{\max}$ possess long tails of rare events with larger values of susceptibility. The samples which correspond to the rare events give a large contribution to the average and shift it far from the most probable values. The value of $\overline{\chi}_{\max}$ calculated with the complete probability distribution is shown in fig. 4 by a dashed line (blue on-line). Another characteristic value shown in fig. 4 by lines (solid) are the median values χ_{med} , defined as the values of χ where the integrated probability distributions are equal to 0.5. A distance between the average and median

values may serve to quantify the asymmetricity of the probability distribution.

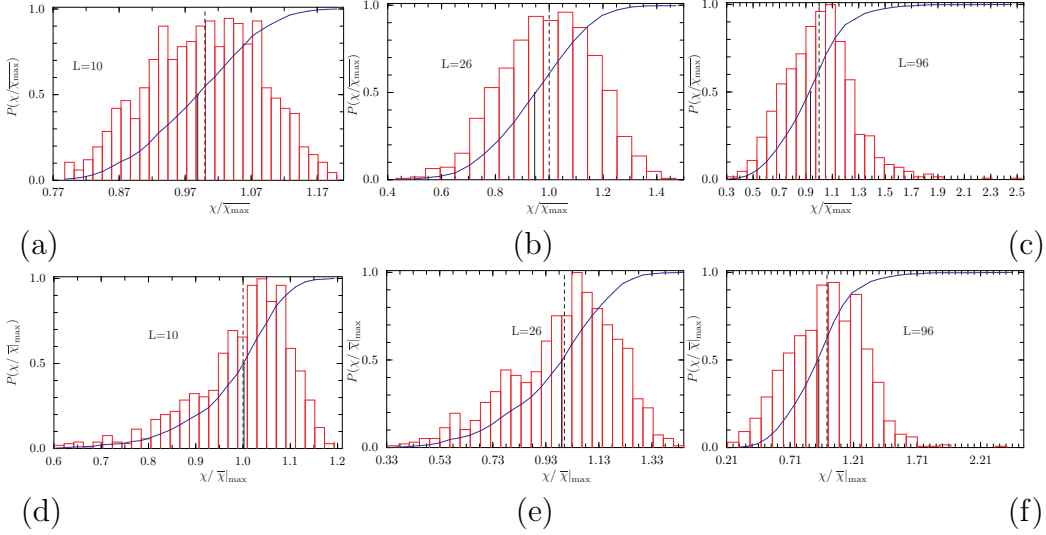


Figure 4. Probability distributions of the susceptibilities $\overline{\chi}_{\max}$, (Fig. 4a-4c) and $\bar{\chi}_{\max}$, (Fig. 4d-4f) for the lattice sizes $L = 10, 26, 96$ (from left to right). The full curves (blue on-line) represent the integrated distribution. Dashed vertical lines (blue on-line) show $\overline{\chi}_{\max}$, and $\bar{\chi}_{\max}$, calculated with the complete probability distribution. Solid lines show the median.

Figures 5 and 6 show contributions of typical and rare events to the temperature behaviour of the observables under discussion. As an example of typical events, we plot in fig. 5 the magnetic susceptibility χ , Binder's cumulant U_4 , and magnetisation $\langle |\mathcal{M}| \rangle$ selecting the samples where susceptibilities have the same values as $\bar{\chi}$ at β_{\max} for the largest lattice size $L = 96$. Few examples of rare events corresponding to large values of χ are shown in Fig. 6. The bold lines in the figures show averages over all disorder realizations (all samples). The thin lines (color on-line) correspond to different samples, as shown in the legends to the plots 5a, 6a.

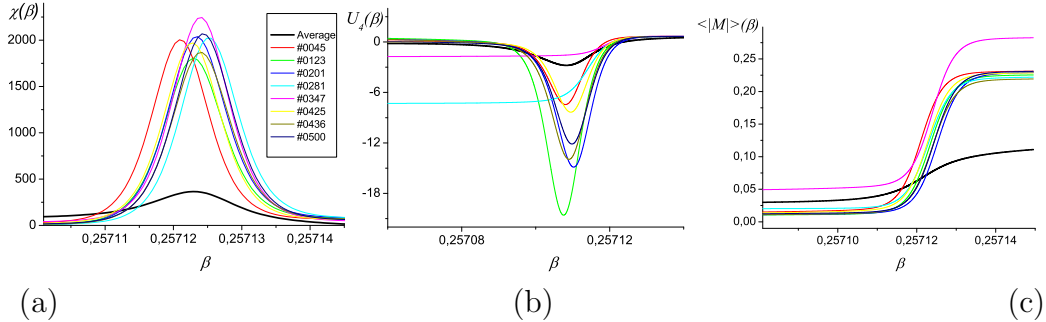


Figure 5. Examples of *typical* events for the largest lattice size $L = 96$ for magnetic susceptibility χ (a), Binder's cumulant U_4 (b) and magnetisation $\langle |\mathcal{M}| \rangle$ (c). Different colours correspond to different samples. The thick lines show the averages (calculated via *averaging b*) over 10^3 samples.

It follows from the above analysis that the rare events are obviously present

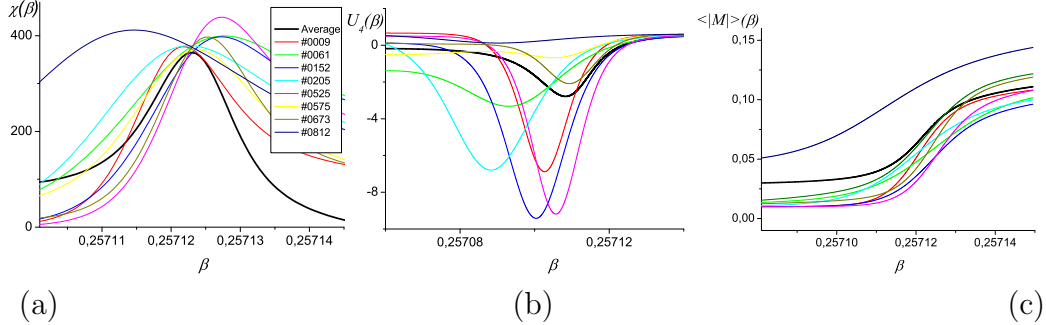


Figure 6. Examples of *rare events* for the largest lattice size $L = 96$ for magnetic susceptibility χ (a), Binder's cumulant U_4 (b) and magnetisation $\langle |\mathcal{M}| \rangle$ (c). Different colours correspond to different samples. The thick lines show the averages over all 10^3 samples.

in the random variables distributions and give a contribution to the average values of physical quantities.²

These are the average values that correspond to the observables and are to be used for for the FSS analysis. We will perform such analysis in the next subsection.

4.2 Evaluation of the critical exponents. Grand canonical disorder

Before passing to evaluation of the critical exponents let us recall that as it was noted at the beginning of section 5 we perform the simulations for the samples with varying concentration of magnetic sites, keeping the mean concentration equal to $p = 0.8$ and limiting dispersion of concentrations by $\sigma^2 = 10^{-4}$ (5). Following Refs. [34] it is natural to call such situation the 'grand canonical disorder'. Afterwards, in section 4.3 we will consider the case of 'canonical disorder', when we will choose the samples much more close in the concentration of magnetic sites (taking $\sigma^2 = 10^{-7}$).

4.2.1 Averaging a

In the finite-size-scaling technique [26], the critical exponents are calculated by fitting the data set for the observables evaluated at various lattice sizes to the power laws (14), (16) as was already mentioned in section 3. This procedure will be used for the evaluation of the critical exponents ν , β , and γ based on the observables measured during the MC simulations. Corresponding

² The use of the familiar 3σ law to choose the samples during the MC experiment (as it was done at the initial phase of our analysis, see Ref. [33]) modifies the distribution. Such modifying leads to different results for the exponents. We thank the referee for the comments on this point.

finite-size-scaling plots are shown in Figs. 7, 8, the numbers are given in table 3. In Fig. 7, we give the log-log plots of the maximum values of the configurationally averaged derivatives of Binder cumulants D_{U_4} and D_{U_2} . The scaling of these quantities is governed by the correlation length critical exponent ν , see Eqs. (14). Fig. 8 shows the size dependence of the configurationally averaged magnetic susceptibility $\overline{\chi_{\max}}$ (Fig. 8a) and magnetisation $\overline{|\mathcal{M}|}_{\max}$ (Fig. 8b). These values are expected to manifest a power-law scaling with exponents β/ν and γ/ν , see Eq. (14).

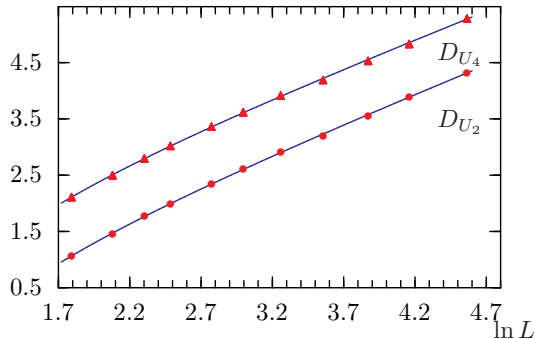


Figure 7. Log-log plots for the maximum values of the configurationally averaged derivatives of Binder cumulants D_{U_2} (discs) and D_{U_4} (triangles). Solid line: data fit to the power law with the correction-to-scaling, Eq. (16). Here and below the range of the confidence interval is smaller than the symbol size.

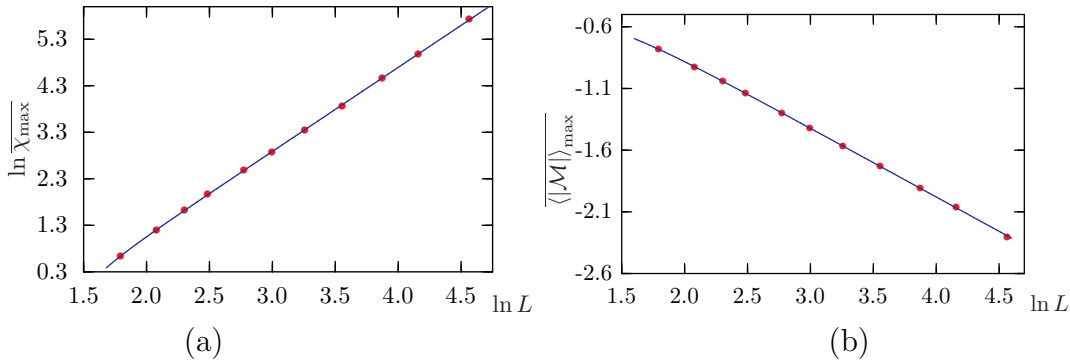


Figure 8. Log-log plots for the configurationally averaged maximum values of the magnetic susceptibility $\overline{\chi_{\max}}$ and magnetisation $\overline{|\mathcal{M}|}_{\max}$. Solid line: data fit to the power law with the correction-to-scaling, Eq. (16).

We used several ways to extract the values of the exponents from the data given in Table 3 and plotted in Figs. 7, 8, an outcome is summarized in the table 4.

First, we used the fit to the power laws (14) for all data points. Resulting exponents are given in the third column of table 4. Having a possibility to estimate ν from the scaling of two different magnetic cumulants, D_{U_2} and D_{U_4} , we give in the table also an average value of ν , $\bar{\nu}$, that results from these estimates. However, such a straightforward estimate of the exponents made for the lattice sizes $L = 6 \div 96$ may be not accurate enough, as far as

	$\overline{\chi_{\max}}$	$\overline{\langle \mathcal{M} \rangle}_{\max}$	D_{U_4}	D_{U_2}
6	1.886 ± 0.003	0.4584 ± 0.0002	8.248 ± 0.007	2.900 ± 0.003
8	3.312 ± 0.007	0.3976 ± 0.0003	12.18 ± 0.02	4.320 ± 0.007
10	5.068 ± 0.013	0.3533 ± 0.0003	16.41 ± 0.04	5.863 ± 0.014
12	7.121 ± 0.023	0.3205 ± 0.0003	20.50 ± 0.06	7.356 ± 0.024
16	11.95 ± 0.05	0.2735 ± 0.0004	28.87 ± 0.13	10.45 ± 0.05
20	17.85 ± 0.08	0.2413 ± 0.0004	37.33 ± 0.23	13.65 ± 0.08
26	28.66 ± 0.14	0.2096 ± 0.0004	50.10 ± 0.49	18.46 ± 0.15
35	48.07 ± 0.28	0.1778 ± 0.0005	66.14 ± 0.71	24.58 ± 0.25
48	86.34 ± 0.55	0.1491 ± 0.0005	92.83 ± 1.05	34.92 ± 0.38
64	147.3 ± 1.0	0.1272 ± 0.0005	125.4 ± 1.9	48.45 ± 0.72
96	310.5 ± 2.6	0.1001 ± 0.0004	197.1 ± 4.5	74.71 ± 1.49

Table 3. MC simulation data obtained for 3d Ising model with long-range correlated disorder: *averaging a.*

Exponents	Observables	Data fit (Number of data points n and value of ω)		
		$n = 11,$ $\omega = 0$	$n = 5,$ $\omega = 0$	$n = 11,$ $\omega = 0.8$
ν	D_{U_4}	0.804(17)	0.968(19)	1.009(15)
ν	D_{U_2}	0.789(16)	0.935(17)	0.977(13)
$\bar{\nu}$	D_{U_4}, D_{U_2}	0.796(12)	0.951(13)	0.993(10)
γ/ν	$\overline{\chi_{\max}}$	1.845(11)	1.825(13)	1.748(16)
β/ν	$\overline{\langle \mathcal{M} \rangle_{\max}}$	0.535(5)	0.560(4)	0.586(5)
$2\beta/\nu + \gamma/\nu$	$\overline{\chi_{\max}}, \overline{\langle \mathcal{M} \rangle_{\max}}$	2.916(15)	2.945(15)	2.916(19)

Table 4

Values of the critical exponents obtained from FSS of different observables via *averaging a*. 3rd and 5th columns: fit to all $n = 11$ data points, 4th column: fit to the 5 last data points.

the correction-to-scaling or crossover effects may be present (for an analysis of crossover effects in a similar context, see Ref. [35]). Indeed, one can see a bending of the curves in Fig. 7 for $L = 6 \div 12$. Taking that correction to scaling is especially pronounced for the small lattice sizes we decided to make a power law fit for five largest lattice sizes only. The results for the exponents are given in the fourth column of table 4. Another way to deal with the correction-to-scaling phenomena is to explicitly take into account the correction-to-scaling term in the fit via formula (16). Using theoretical estimate for the correction-to-scaling exponent of the 3d Ising model with long-range-correlated disorder at the value of correlation parameter (see Eq. (1)) $a = 2$, $\omega(a = 2) = 0.8$ [23] and fitting all data points by the formula (16) we arrive at the values of the exponents given in the last column of table 4. An alternative way may be to keep the value of the exponent ω as a fit parameter and fit all data points to Eq. (16) to ensure the same value of the leading exponent as those, obtained from the fit of data for five largest lattice sizes. As we have checked such a procedure leads to the values of exponent ω in the reasonable agreement with the theoretical estimate $\omega = 0.8$ [23].

Comparing data for the exponents obtained by a power law fit (14) for five last data points (five largest lattice sizes) with the data obtained by a fit of all data points to the expression that takes into account the correction-to-scaling exponent, Eq. (16), we arrive to self-consistent results. Indeed, as one can see from the table 4, the average value of the correlation length exponent lies in the interval $\bar{\nu} = 0.95 \div 0.99$, the other exponents are in the range $\gamma/\nu = 1.75 \div 1.83$, $\beta/\nu = 0.54 \div 0.58$. Another check of the accuracy of the results obtained is the value of the combination of the exponents $2\beta/\nu + \gamma/\nu$ which is to be

equal to three by a hyperscaling relation $2\beta + \gamma = d\nu$. These value is given in the last row of the table.

4.2.2 Averaging b

Now let us carry out analysis being based on the same samples but to perform an averaging we will use the procedure described above as an *averaging b*. Results of the analysis are summarized in tables 5, 6 and Figures 9, 10. Similarly as in the former subsection 4.2.1 we give in the table 5 the values of the observables that are used in the FSS analysis. Now one can extract the correlation length critical exponent ν from the FSS of maxima of four different quantities: temperature derivatives of logarithm of magnetization and of its square \mathcal{D}_M , \mathcal{D}_{M^2} (12) and of magnetic cumulants \mathcal{D}_{U_4} , \mathcal{D}_{U_2} (10). Corresponding plots are given in fig. 9. Again as in the former subsection we used different ways to fit data points to the power law dependence. On the one hand, we used simple power law (15), on the other hand, the correction-to-scaling was taken into account via formula (16).

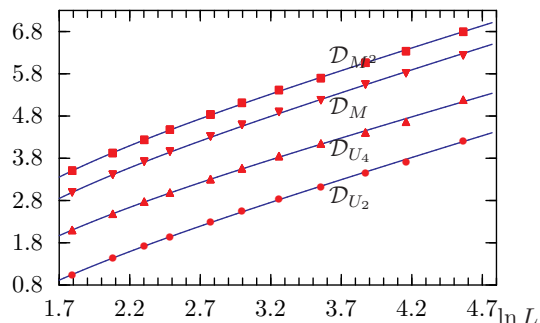


Figure 9. Log-log plots for the maximum values of the configurationally averaged derivatives of Binder cumulants \mathcal{D}_{U_2} (discs), \mathcal{D}_{U_4} (triangles up), \mathcal{D}_M (triangles down) and \mathcal{D}_{M^2} (squares). Solid line: data fit to the power law with the correction-to-scaling, Eq. (16).

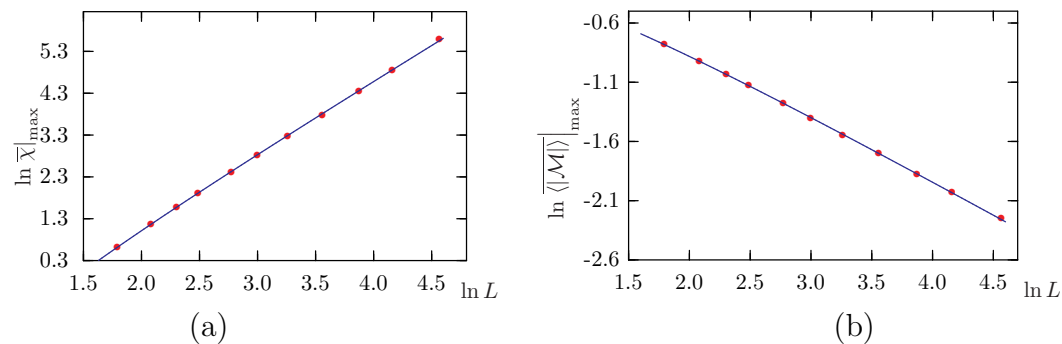


Figure 10. Log-log plots for the configurationally averaged maximum values of the magnetic susceptibility $\bar{\chi}_{\max}$ and magnetisation $\overline{\langle |\mathcal{M}| \rangle}_{\max}$. Solid line: data fit to the power law with the correction-to-scaling, Eq. (16).

	$\bar{\chi} _{\max}$	$\overline{\langle \mathcal{M} \rangle} _{\max}$	\mathcal{D}_{U_4}	\mathcal{D}_{U_2}	\mathcal{D}_M	\mathcal{D}_{M^2}
6	1.850 ± 0.003	0.4583 ± 0.0006	8.178 ± 0.001	2.850 ± 0.001	19.958 ± 0.007	33.248 ± 0.013
8	3.205 ± 0.008	0.3974 ± 0.0006	11.98 ± 0.01	4.189 ± 0.003	30.269 ± 0.005	50.630 ± 0.051
10	4.872 ± 0.016	0.3564 ± 0.0005	15.99 ± 0.03	5.641 ± 0.012	41.245 ± 0.059	68.993 ± 0.159
12	6.806 ± 0.026	0.3245 ± 0.0002	19.73 ± 0.05	7.003 ± 0.019	52.326 ± 0.102	87.714 ± 0.235
16	11.27 ± 0.054	0.2792 ± 0.0002	27.29 ± 0.11	9.807 ± 0.042	74.989 ± 0.238	125.94 ± 0.47
20	16.65 ± 0.089	0.2474 ± 0.0002	35.22 ± 0.19	12.77 ± 0.066	98.707 ± 0.388	165.89 ± 0.72
26	26.32 ± 0.157	0.2147 ± 0.0003	47.06 ± 0.24	17.20 ± 0.10	133.97 ± 0.63	225.22 ± 1.14
35	43.45 ± 0.304	0.1837 ± 0.0004	58.63 ± 0.44	22.02 ± 0.18	177.58 ± 1.05	299.58 ± 1.75
48	77.51 ± 0.583	0.1535 ± 0.0005	84.83 ± 0.08	31.81 ± 0.22	256.23 ± 1.55	431.99 ± 2.67
64	128.8 ± 1.073	0.1314 ± 0.0006	105.8 ± 0.9	41.05 ± 0.38	335.01 ± 2.34	565.50 ± 3.73
96	269.0 ± 2.457	0.1061 ± 0.0006	178.4 ± 1.2	67.75 ± 0.49	588.48 ± 3.01	1012.7 ± 4.4

Table 5. MC simulation data obtained for 3d Ising model with long-range correlated disorder: *averaging b*.

The values of the exponent ν for different fits are given in the Table 6. Having defined ν from the scaling of four different quantities (\mathcal{D}_{U_4} , \mathcal{D}_{U_2} , \mathcal{D}_M , \mathcal{D}_{M^2}) we find also an average value on ν , $\bar{\nu}$, and quote it in the table as well. Similarly, from the log-log dependence of $\bar{\chi}|_{\max}$ and $\overline{\langle |\mathcal{M}| \rangle}|_{\max}$ (shown in fig. 10) we extract values of the exponents γ/ν and β/ν , see Eq. (15). Again the values of the exponents that result from different fits are shown in Table 6.

Exponents	Observables	Data fit (Number of data points n and value of ω)		
		$n = 11,$ $\omega = 0$	$n = 5,$ $\omega = 0$	$n = 11,$ $\omega = 0.8$
ν	\mathcal{D}_{M^2}	0.796(20)	0.946(13)	0.989(11)
ν	\mathcal{D}_M	0.754(24)	0.970(16)	0.977(14)
ν	\mathcal{D}_{U_4}	0.827(20)	1.006(43)	1.051(18)
ν	\mathcal{D}_{U_2}	0.816(18)	0.960(29)	1.002(15)
$\bar{\nu}$	$\mathcal{D}_{U_4}, \mathcal{D}_{U_2}, \mathcal{D}_M, \mathcal{D}_{M^2}$	0.798(10)	0.971(14)	1.005(7)
γ/ν	$\bar{\chi} _{\max}$	1.802(12)	1.779(14)	1.699(16)
β/ν	$\overline{\langle \mathcal{M} \rangle} _{\max}$	0.525(4)	0.540(6)	0.567(5)
$2\beta/\nu + \gamma/\nu$	$\bar{\chi} _{\max}, \overline{\langle \mathcal{M} \rangle} _{\max}$	2.852(14)	2.859(18)	2.833(19)

Table 6

Values of the critical exponents obtained from FSS of different observables via *averaging b*. 3rd and 5th columns: fit to all $n = 11$ data points, 4th column: fit to the 5 last data points.

As it was observed already in section 4.2.1, the strong correction-to-scaling occurs for the small lattice sizes. Similar phenomenon happens when one applies procedure of *averaging b*. An evidence may serve the bending of the curves in Fig. 9 for the small L . Therefore we conclude that the most reliable numerical data is obtained either from the FSS of five largest lattices or from all data points but with an account of the correction-to-scaling exponents. From table 6 we conclude that the exponent lays in the range $\bar{\nu} = 0.97 \div 1.01$, $\gamma/\nu = 1.70 \div 1.78$, $\beta/\nu = 0.54 \div 0.57$.

Tables 4 and 6 summarize results for the exponents obtained via different averaging procedures (*a* and *b*) and via different fitting procedures for the same samples. Recall that preparing the samples we have kept an average value of magnetic sites concentration fixed and equal to $p = 0.8$ with the dispersion $\sigma^2 = 10^{-4}$. The next step in our analysis will be to check how does the concentration fluctuations influence the values of the (thermodynamical) critical exponents.

4.3 Evaluation of the critical exponents. Canonical disorder

Let us consider now the situation when the dispersion of concentration p is much smaller as it was taken in the former subsection. that is, keeping the same average concentration of magnetic sites $p = 0.8$ let us consider much more narrow distribution of its values for separate samples. For the study, performed in this subsection we take the dispersion to be $\sigma^2 = 10^{-7}$. Doing so we introduce 'canonical disorder' in the spirit of Ref. [34]. As we will see below, this step is also can serve as an separate independent check of the values of the critical exponents we are interested in.

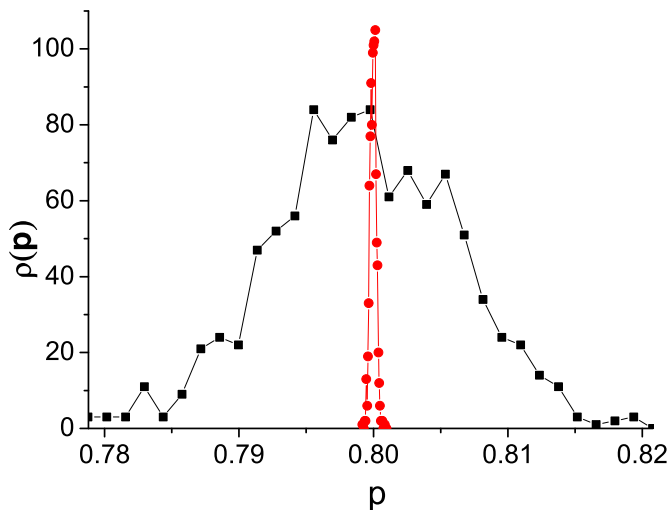


Figure 11. Distribution function $\rho(p)$ of the magnetic spin concentration p for 'grand canonical disorder' and 'canonical disorder' in comparison, ($L = 96$).

Similarly as it was described above, we perform an averaging over disorder in two different ways, via *averaging a* and *averaging b*. We extract the values of the exponents by the FSS dependence of different observables as explicitly given in Eqs. (14) - (16). Intermediate results and log-log plots of these observables as functions of the lattice size are given in Appendices A and B. The data for the exponents are summarized in the tables 7 and 8 for averaging *a* and *b*, respectively.

Comparing data of tables 4 and 6 with the data of tables 7 and 8 ones can see that the values of the exponents depend on the way the averaging over disorder was performed (*averaging a* and *b*) as well as on the way the disorder was prepared (grand canonical and canonical disorder). In particular, passing from the grand canonical disorder to the canonical disorder one observes an increase of γ/ν and decrease of β/ν . This difference in the exponents is more pronounced for the *averaging a* (of order of 8 %) and less pronounced for the

Exponents	Observables	Data fit (Number of data points n and value of ω)		
		$n = 12,$ $\omega = 0$	$n = 5,$ $\omega = 0$	$n = 12,$ $\omega = 0.8$
ν	D_{U_4}	0.841(15)	0.887(31)	0.989(15)
ν	D_{U_2}	0.817(16)	0.904(19)	0.975(12)
$\bar{\nu}$	D_{U_4}, D_{U_2}	0.829(11)	0.896(18)	0.982(10)
γ/ν	$\overline{\chi_{\max}}$	1.868(12)	1.999(33)	1.857(40)
β/ν	$\overline{\langle \mathcal{M} \rangle}_{\max}$	0.526(2)	0.527(2)	0.538(9)
$2\beta/\nu + \gamma/\nu$	$\overline{\chi_{\max}}, \overline{\langle \mathcal{M} \rangle}_{\max}$	2.920(13)	3.053(33)	2.933(44)

Table 7

Values of the critical exponents obtained from FSS of different observables via *averaging a*. 3rd and 5th columns: fit to all $n = 12$ data points, 4th column: fit to the 5 last data points.

Exponents	Observables	Data fit (Number of data points n and value of ω)		
		$n = 12,$ $\omega = 0$	$n = 5,$ $\omega = 0$	$n = 12,$ $\omega = 0.8$
ν	\mathcal{D}_{M^2}	0.807(13)	0.834(20)	0.932(12)
ν	\mathcal{D}_M	0.764(18)	0.866(18)	0.956(12)
ν	\mathcal{D}_{U_4}	0.855(7)	0.958(13)	0.991(8)
ν	\mathcal{D}_{U_2}	0.841(18)	0.921(21)	1.031(17)
$\bar{\nu}$	$\mathcal{D}_{U_4}, \mathcal{D}_{U_2}, \mathcal{D}_M, \mathcal{D}_{M^2}$	0.817(7)	0.895(7)	0.978(6)
γ/ν	$\overline{\chi}_{\max}$	1.800(12)	1.834(19)	1.731(27)
β/ν	$\overline{\langle \mathcal{M} \rangle}_{\max}$	0.516(5)	0.528(12)	0.562(4)
$2\beta/\nu + \gamma/\nu$	$\overline{\chi}_{\max}, \overline{\langle \mathcal{M} \rangle}_{\max}$	2.832(16)	2.890(31)	2.855(28)

Table 8

Values of the critical exponents obtained from FSS of different observables via *averaging b*. 3rd and 5th columns: fit to all $n = 12$ data points, 4th column: fit to the 5 last data points.

averaging b (of order of 2-4 %). Deviation in the exponent ν is of order of 5 %. We further compare these values with the other data available and make some conclusions in the next section.

5 Conclusions and outlook

As we explained in the introduction, our paper was inspired by existing contradictory results about the critical behaviour of the 3d Ising model with long-range-correlated impurities. Whereas both theoretical and MC studies [5, 12, 13, 15, 16] agree about the new universality class that arises in such a model, there exist an essential disagreement between the estimates for the critical exponents. For the value of the impurity correlation parameter $a = 2$ they are summarized in table 1. The numerical data obtained so far split into two groups giving essentially different results for the exponents. To give an example, the predicted value for the correlation length critical exponent ν deviates between these groups within order of 30 % ranging from $\nu = 1$ [5, 15] to $\nu \simeq 0.71$ [12, 16].

To resolve existing contradictions, we performed MC simulations of the 3d Ising model with long-range-correlated disorder in a form of randomly oriented lines of non-magnetic sites (impurity lines). Concentration of the impurities was taken to be $1 - p = 0.2$. We used different ways to perform an averaging over disorder realizations, referred as *averaging a* and *averaging b*. Moreover, we used two different ways to prepare the samples: in one case we allowed for a wide distribution of concentration (grand canonical disorder) and the other case we made this distribution very narrow (canonical disorder). Swendsen-Wang MC algorithm and a finite-size-scaling analysis were applied to extract values of the critical exponents that govern magnetic phase transition in such a system. Our estimates for the critical exponents ν , β , and γ are given in tables 4, 6, 7, 8. As we have discussed above, the most reliable data fits have been obtained by fitting the whole data for a given observable set taking into account the correction-to-scaling exponent or by fitting the data for the largest lattice sizes to the asymptotic scaling behaviour. These results are summarized in table 9.

One can see from the table, that different ways to perform (and to analyze) the simulation lead to slightly different values of the exponents. Whereas technical reasons for such deviations are obvious, there is no physical reason for them. That is all cases considered should correspond to the same asymptotic behaviour of physical quantities. Moreover, if in a simulation only one case were considered, there would be no way to see such deviation. Therefore, we find it reasonable to look for the averaged values of the exponents, as given in the last column of the table 9

$$\nu = 0.958 \pm 0.004, \quad \gamma/\nu = 1.809 \pm 0.009, \quad \beta/\nu = 0.551 \pm 0.002. \quad (17)$$

Comparing our data quoted in table 9 with those previously obtained, table 1, one sees that our analysis leads to the results differing from the existing

Exponents	grand canonical disorder				canonical disorder				Averaged value
	<i>averaging a</i>		<i>averaging b</i>		<i>average a</i>		<i>average b</i>		
	$n = 5,$ $\omega = 0$	$n = 11,$ $\omega = 0.8$	$n = 5,$ $\omega = 0$	$n = 11,$ $\omega = 0.8$	$n = 5,$ $\omega = 0$	$n = 12,$ $\omega = 0.8$	$n = 5,$ $\omega = 0$	$n = 12,$ $\omega = 0.8$	
$\bar{\nu}$	0.951(13)	0.993(10)	0.971(14)	1.005(7)	0.892(18)	0.982(10)	0.895(7)	0.978(6)	0.958(4)
γ/ν	1.825(13)	1.748(16)	1.779(14)	1.699(16)	1.999(33)	1.857(40)	1.834(19)	1.731(27)	1.809(9)
β/ν	0.560(4)	0.586(5)	0.540(6)	0.567(5)	0.527(2)	0.538(9)	0.528(12)	0.562(4)	0.551(2)
$2\beta/\nu + \gamma/\nu$	2.945(15)	2.916(19)	2.859(18)	2.833(19)	3.053(33)	2.933(44)	2.890(31)	2.855(28)	2.911(10)

Table 9. Values of the critical exponents obtained via *averaging a* and *averaging b* for the grand canonical and for the canonical disorder. The last column gives averaged values.

so far and therefore on the first sight does not make the situation more clear. However, we want to emphasize several items, opposing our results to previous theoretical and numerical estimates.

As first discussed in Ref. [12], a difference between existing theoretical estimates for the exponents is caused by the fact that the renormalization group analysis of Weinrib and Halperin [5] was performed in the first order of the perturbation theory with subsequent conjecture that the first order result $\nu = 2/a$ is exact. Upcoming two-loop calculations at $d = 3$ [12] gave numerical results for the exponents which disagree with this conjecture and question it. Although one may consider this result as a signal about non-trivial dependence of the exponents on the disorder correlation parameter a (as well as on the order parameter dimension), one certainly should not take the numbers obtained as a final estimates of the exponents. Indeed in the renormalization group theory of disordered systems, and, more general, of systems described by effective Hamiltonians of complicated symmetry, one finds many examples when the two-loop numerical estimates are essentially improved by higher-order contributions (see e.g. reviews [1] and references therein). In support to this suggestion let us point to the fact, that the two-loop theoretical estimates of Ref. [12] bring about the negative sign for the pair correlation function critical exponent η (see table 1), whereas for the ϕ^4 theory the positiveness of η follows from the Källen-Lhemann decomposition. Therefore, our results for the exponents support general scenario found in Ref. [12], whilst the numerical discrepancy may be explained by possible changes in the theoretical estimates due to the high-order contributions.

Another question concerns discrepancies between the results of numerical simulations of the 3d Ising model with long-range correlated disorder at $a = 2$ [15, 16]. In Ref. [16] the discrepancies were explained by the differences in the objects of simulation: in the simulations of Ballesteros et al. [15] the impurity lines were allowed to intersect opposite to the mutually avoiding impurity lines considered in the simulations of Prudnikov et al. [12]. One way to check whether the above difference in the impurity distributions causes any influence on the magnetic subsystem critical behaviour is to analyze an asymptotics of the function $g(r)$ (1). As it follows from our analysis [32], both distributions lead to the power law asymptotics (1) with close values of $a \simeq 2$. This observation gives an evidence of the fact that both disorder distributions lead to the same values of the exponents. At least, if the difference exists it can not be seen for the system sizes considered. Moreover, if it exists it can not suffice to explain the observed discrepancy between simulations [15] and [16]. Indeed, the former simulations were performed also for the appropriately distributed impurity sites (so-called Gaussian disorder, see section 1), when the very notion of the impurity lines and their intersections loses its sense.

Let us point another phenomenon where the results obtained here may find

possible interpretation. For liquids, a porous medium is often better fitted to the extended long-range-correlated structures [36,37]. To give an example, experiments on ^4He embedded in silica aerogels and xerogels report a change in the universality class [38] which signals about a presence of long-range correlations between defects. Simple fluids immersed in the porous media of certain type (determined by the density-density pair correlation function of form of Eq. (1)) should manifest critical behaviour in the universality class of the 3d Ising model with long-range-correlated disorder. Reported so far values of the critical exponents for the 3d Ising model with defects in a form of a porous medium [19, 39] were rather interpreted in terms of the random-site uncorrelated disorder (note however a numerical agreement between the results of Ref. [39] and our estimates). We hope that our simulations will attract more attention to the interpretation of experimental and numerical studies of criticality of liquids in porous medium in terms of long-range-correlated disorder considered here.

Let us return back to the values of the exponents quoted in the last column of table 9. From this data one gets the following values of the magnetic susceptibility and magnetization critical exponents: $\gamma = 1.733(11)$, $\beta = 0.528(3)$. Comparing these values with the results of former MC simulation of Ballesteros and Parisi [15] (c.f. Table 1) one can see that our result for β nicely coincide however the value for γ differs of the order of 13 %, the difference in ν being less dramatic. Note however that our results are in much worse agreement with the simulations of Prudnikov et al. [16]. We do not see any obvious explanation for the discrepancies between MC numerical estimates of the critical behaviour of the 3d random Ising model with long-range-correlated disorder obtained so far and those obtained in our study. Eventually, if we are allowed to make a “not very serious” statement, we must confess that we simply ignore the reasons of the discrepancy between previously available MC simulations and those presented in this work. All three studies seem equally rigorous, but eventually our analysis provides results for the critical exponents which stand between former determinations, and this may be seen as a wise behaviour!

The authors acknowledge useful discussions with Christophe Chatelain and Wolfhard Janke. We are especially thankful to the unknown referee for illuminating comments (that made our simulations even more time consuming). Yu. H. acknowledges support of the FWF project P 19583-PHY.

References

- [1] A. Pelissetto, E. Vicari, Phys. Rep. **368** (2002) 549; R. Folk, Yu. Holovatch, T. Yavors’kii, Phys. Usp. **46** (2003) 169 [Uspekhi Fiz. Nauk **173** (2003) 175]; Order,

- Disorder and Criticality. Advanced Problems of Phase Transition Theory. Ed. by Yuriy Holovatch. World Scientific, Singapore, 2004; vol. 2 - 2007.
- [2] R. Balian, M. Kleman, J. Poirier, Physics of Defects - Les Houches, 1980, North Holland, Amsterdam, 1981.
 - [3] B. M. McCoy, T. T. Wu, Phys. Rev. **176** (1968) 631; B. M. McCoy, Phys. Rev. **188** (1969) 1014.
 - [4] Dorogovtsev S. M. // Fiz. Tverd. Tela (Leningrad) — 1980. — V. 22. — P. 321 [Sov. Phys.–Solid State — 1980. — V. 22. — P. 188]; Dorogovtsev S. M. // Fiz. Tverd. Tela (Leningrad) — 1980. — V. 22. — P. 3659 [Sov. Phys.–Solid State — 1980. — V. 22. — P. 2141].
 - [5] A. Weinrib, B. I. Halperin, Phys. Rev. B **27** (1983) 413.
 - [6] J. C. Lee, R. L. Gibbs, Phys. Rev. B **45** (1992) 2217; L. De Cesare, Phys. Rev. B **49** (1994) 11742; A. L. Korzhenevskii, K. Herrmanns, W. Schirmacher, Phys. Rev. B **53** (1996) 14834.
 - [7] D. Boyanovsky, J. L. Cardy, Phys. Rev. B **26** (1982) 154; Erratum: Phys. Rev. B **27** (1983) 6971.
 - [8] I. D. Lawrie, V. V. Prudnikov, J. Phys. C **17** (1984) 1655.
 - [9] Y. Yamazaki, A. Holz, M. Ochiai, Y. Fukuda, Phys. Rev. B **33** (1986) 3460; Physica A **136** (1986) 303; Y. Yamazaki, M. Ochiai, A. Holz, Y. Fukuda, Phys. Rev. B **33** (1986) 3474; Y. Yamazaki, A. Holz, M. Ochiai, Y. Fukuda, Physica A **150** (1988) 576.
 - [10] A. A. Fedorenko, Phys. Rev. B **69** (2004) 134301.
 - [11] V. Blavats'ka, C. von Ferber, Yu. Holovatch, Phys. Rev. B. **67** (2003) 094404; V. Blavats'ka, M. Dudka, R. Folk, Yu. Holovatch, Phys. Rev. B **72** (2005) 064417.
 - [12] V. V. Prudnikov, P. V. Prudnikov, A. A. Fedorenko, J. Phys. A **32** (1999) L399; V. V. Prudnikov, P. V. Prudnikov, A. A. Fedorenko, J. Phys. A **32** (1999) 8587; V. V. Prudnikov, P. V. Prudnikov, A. A. Fedorenko, Phys. Rev. B **62** (2000) 8777.
 - [13] E. Korutcheva, D. Uzunov, Phys. Status Solidi B **126**, K19 (1984); E. Korutcheva, F. Javier de la Rubia, Phys. Rev. B **58**, 5153 (1998).
 - [14] T. Vojta, J. Phys. A **36** (2003) 10921; R. Sknepnek, T. Vojta, Phys. Rev. B **69** (2004) 174410; T. Vojta, J. Phys. A **39** (2006) R143.
 - [15] H. G. Ballesteros, G. Parisi G., Phys. Rev. B **60** (1999) 12912.
 - [16] V. V. Prudnikov, P. V. Prudnikov, S. V. Dorofeev, V. Yu. Kolesnikov, Condens. Matter Phys. **8** (2005) 213; V. Prudnikov, P. Prudnikov, B. Zheng, S. Dorofeev, V. Kolesnikov, Progr. Theor. Phys. **117** (2007) 973.
 - [17] F. Á. Bagaméry, L. Turban, F. Iglói, Phys. Rev. B **72** (2005) 094202.

- [18] A. B. Harris, J. Phys. C **7** (1974) 1671.
- [19] Vásquez C. Estudio sistemático de la influencia del desorden en transiciones de fase: thesis. / C. Vásquez — IVIC, Venezuela, 2003; Vásquez C.R. New universality class for the three-dimensional XY model with correlated impurities: application to ^4He in aerogels / C. Vásquez R., R. Paredes V., A. Hasmy et al. // Phys. Rev. Lett. — 2003. — V. 90. — P. 170602; Vásquez C. Effects of aerogel-like disorder on the critical behavior of $O(m)$ -vector models. Recent simulations and experimental evidence / C. Vásquez, R. Paredes // Condens. Matter Phys. — 2006. — V. 9. No. 2(46). — P. 305–317; Paredes R.V. Three-dimensional Ising model confined in low-porosity aerogels: A Monte Carlo study / R. Paredes V., C. Vásquez // Phys. Rev. B — 2006. — V. 74. — P. 054201.
- [20] Nicolaidis D. Critical behavior in systems with a long-range correlated frozen-in random field / D. Nicolaidis // Phys. Rev. B — 2000. — V. 61. — P. 246.
- [21] Weinrib A. Long-range correlated percolation / A. Weinrib // Phys. Rev. B — 1984. — V. 29. — P. 387–395.
- [22] V. Blavats'ka, C. von Ferber, R. Folk, Yu. Holovatch, in: Statistics of Linear Polymers in Disordered Media, Ed. by Bikas K. Chakrabarti, Elsevier, Amsterdam, 2005; V. Blavats'ka, C. von Ferber, Yu. Holovatch, Phys. Rev. E **74** (2006) 031801.
- [23] V. Blavats'ka, C. von Ferber, Yu. Holovatch, Phys. Rev. E **64** (2001) 041102.
- [24] F. Iglói, C. Monthus, Phys. Rep. **412** (2005) 277.
- [25] R. Guida, J. Zinn-Justin, J. Phys. A **31** (1998) 8103.
- [26] A. M. Ferrenberg, D. P. Landau, Phys. Rev. B **44** (1991) 5081.
- [27] W. Janke, R. Villanova, Phys. Lett. A **209** (1995) 179 (1995); Phys. Rev. B **66** (2002) 134208.
- [28] H. G. Ballesteros, L. A. Fernández, V. Martín-Mayor, A. Muñoz Sudupe, G. Parisi, J. J. Ruiz-Lorenzo, Phys. Rev. B **58** (1998) 175.
- [29] D. Ivaneyko, J. Ilnytskyi, B. Berche B., Yu. Holovatch, Condens. Matter Phys. **8** 149, (2005).
- [30] D. Ivaneyko, J. Ilnytskyi, B. Berche, Yu. Holovatch, Physica A **370** (2006) 163; D. Ivaneyko, J. Ilnytskyi, B. Berche, Yu. Holovatch, J. Mol. Liq. **127** (2006) 69.
- [31] P.E. Berche, C. Chatelain, B. Berche and W. Janke, Eur. Phys. J. B **38** (2004) 463; C. Chatelain, B. Berche, W. Janke and P.E. Berche, Nucl. Phys. B **719** (2005) 275; W. Janke, B. Berche, C. Chatelain, P.E. Berche, M. Hellmund, PoS (LAT2005) 018 (<http://pos.sissa.it/archive/conferences/020/018/>).
- [32] D. Ivaneyko, B. Berche, Yu. Holovatch, J. Ilnytskyi, Problems in Atomic Science and Technology, Ser. Nuclear Physics, No 3(2) (2007) 372. [arXiv:cond-mat/0611778v1].

- [33] D. Ivaneyko, B. Berche, Yu. Holovatch, J. Ilnytskyi, arXiv:cond-mat/0611568v1.
- [34] S. Wiseman, E. Domany, Phys. Rev. Lett. **81** (1998) 22; A. Aharony, A.B. Harris, S. Wiseman, Phys. Rev. Lett. **81** (1998) 252; S. Wiseman, E. Domany, Phys. Rev. E **58** (1998) 2938.
- [35] P.E. Berche, C. Chatelain, B. Berche, W. Janke, Comp. Phys. Comm. **147** (2002) 427; B. Berche, P.E. Berche, C. Chatelain, W. Janke, Condens. Matter Phys. **8** (2005) 47.
- [36] B. K. Chakrabarti, Statistics of Linear Polymers in Disordered Media (Elsevier, Amsterdam, 2005).
- [37] Proceedings of the IV Int. Symp. on Aerogels, J. Non-Cryst. Solids 186 (1995).
- [38] M. H. W. Chan, K. I. Blum, S. Q. Murphy, G. K. S. Wong, J. D. Reppy, Phys. Rev. Lett. **61** (1988) 1950; J. Yoon, D. Sergatskov, J. Ma, N. Mulders, M. H. W. Chan, Phys. Rev. Lett. **80** (1998) 1461.
- [39] T. MacFarland, G. T. Barkema, J. F. Marko, Phys. Rev. B **53** (1996) 148.

Appendix A

In this appendix, we give data obtained via *averaging a* during MC simulations for the canonical disorder, as explained at the beginning of section 4.3. In table 10 we give numerical values of maxima of averaged quantities $\overline{\chi_{\max}}$, $\langle |\mathcal{M}| \rangle_{\max}$, D_{U_4} , and D_{U_2} , Eq. (10). Log-log plots of the dependence of these quantities on the lattice size L are given in Figs. 12 and 13.

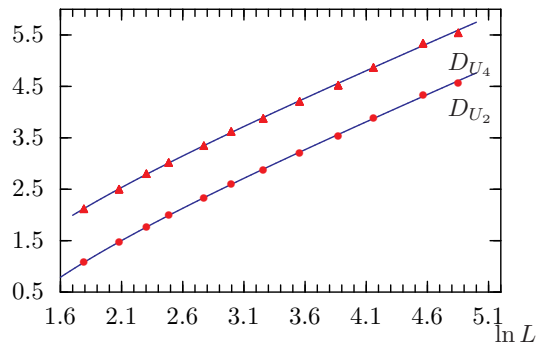


Figure 12. Log-log plots for the maximum values of the configurationally averaged derivatives of Binder cumulants D_{U_2} (discs) and D_{U_4} (triangles). Solid line: data fit to the power law with the correction-to-scaling, Eq. (16).

	$\overline{\chi_{\max}}$	$\overline{\langle \mathcal{M} \rangle}_{\max}$	D_{U_4}	D_{U_2}
6	1.875 ± 0.003	0.4572 ± 0.0002	8.323 ± 0.007	2.937 ± 0.003
8	3.281 ± 0.007	0.3947 ± 0.0003	12.20 ± 0.02	4.338 ± 0.007
10	5.067 ± 0.014	0.3520 ± 0.0003	16.47 ± 0.04	5.895 ± 0.015
12	7.103 ± 0.023	0.3197 ± 0.0003	20.48 ± 0.07	7.354 ± 0.024
16	11.89 ± 0.05	0.2726 ± 0.0003	28.39 ± 0.13	10.28 ± 0.05
20	17.94 ± 0.08	0.2415 ± 0.0004	37.45 ± 0.23	13.59 ± 0.09
26	28.09 ± 0.14	0.2072 ± 0.0005	48.30 ± 0.40	17.80 ± 0.15
35	47.45 ± 0.29	0.1810 ± 0.0010	67.18 ± 0.73	24.50 ± 0.26
48	86.64 ± 0.58	0.1531 ± 0.0005	92.19 ± 0.45	34.56 ± 0.24
64	147.8 ± 1.1	0.1319 ± 0.0005	130.0 ± 1.9	48.67 ± 0.77
96	360.0 ± 2.5	0.1060 ± 0.0006	207.6 ± 1.5	75.81 ± 0.61
128	624.2 ± 4.0	0.0915 ± 0.0004	255.0 ± 4.9	96.69 ± 2.14

Table 10. MC simulation data obtained for 3d Ising model with long-range correlated disorder: *averaging a.*

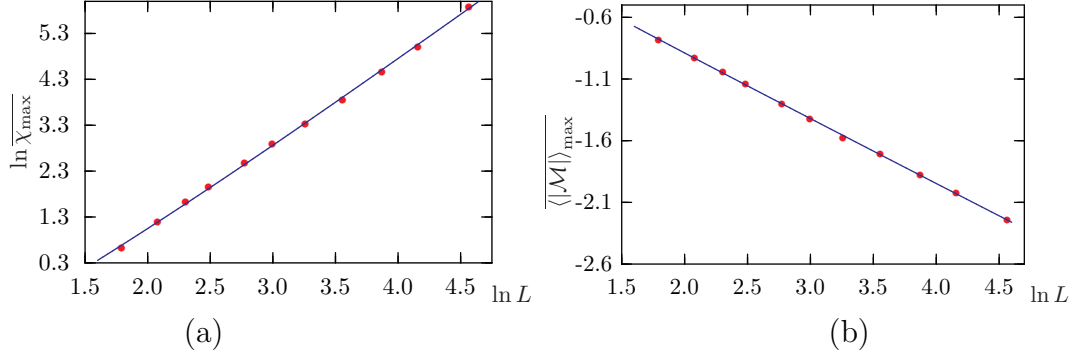


Figure 13. Log-log plots for the configurationally averaged maximum values of the magnetic susceptibility $\bar{\chi}_{\max}$ and magnetisation $\langle |\mathcal{M}| \rangle_{\max}$. Solid line: data fit to the power law with the correction-to-scaling, Eq. (16).

Appendix B

In this appendix, we give data obtained via *averaging* b during MC simulations for the canonical disorder, as explained at the beginning of section 4.3. In table 11 we give numerical values of maxima of averaged quantities $\bar{\chi}|_{\max}$, $\langle |\mathcal{M}| \rangle|_{\max}$, \mathcal{D}_{U_4} , \mathcal{D}_{U_2} , \mathcal{D}_M , \mathcal{D}_{M^2} , Eqs. (11), (12). Log-log plots of the dependence of these quantities on the lattice size L are given in Figs. 14 and 15.

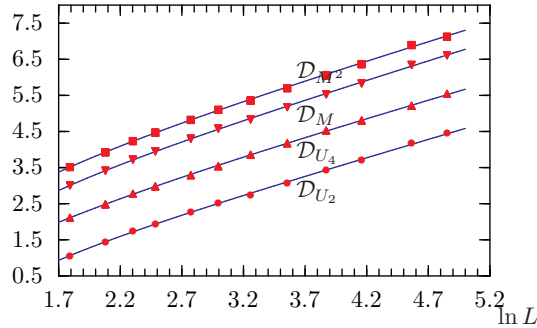


Figure 14. Log-log plots for the maximum values of the configurationally averaged derivatives of Binder cumulants \mathcal{D}_{U_2} (discs), \mathcal{D}_{U_4} (triangles up), \mathcal{D}_M (triangles down) and \mathcal{D}_{M^2} (squares). Solid line: data fit to the power law with the correction-to-scaling, Eq. (16).

	$\bar{\chi} _{\max}$	$\overline{ \mathcal{M} } _{\max}$	\mathcal{D}_{U_4}	\mathcal{D}_{U_2}	\mathcal{D}_M	\mathcal{D}_{M^2}
6	1.848 ± 0.003	0.4575 ± 0.0003	8.258 ± 0.002	2.896 ± 0.001	20.211 ± 0.002	33.623 ± 0.018
8	3.190 ± 0.008	0.3959 ± 0.0004	11.99 ± 0.01	4.217 ± 0.005	30.361 ± 0.012	50.713 ± 0.060
10	4.854 ± 0.016	0.3545 ± 0.0005	16.00 ± 0.03	5.647 ± 0.012	41.256 ± 0.045	69.040 ± 0.134
12	6.806 ± 0.026	0.3241 ± 0.0002	19.67 ± 0.06	6.979 ± 0.022	51.973 ± 0.115	87.095 ± 0.263
16	11.27 ± 0.05	0.2788 ± 0.0002	26.86 ± 0.10	9.636 ± 0.040	73.721 ± 0.229	123.84 ± 0.46
20	16.74 ± 0.09	0.2478 ± 0.0004	34.42 ± 0.16	12.50 ± 0.07	97.287 ± 0.370	163.54 ± 0.68
26	25.71 ± 0.16	0.2150 ± 0.0006	47.22 ± 0.15	15.69 ± 0.10	125.62 ± 0.62	211.95 ± 1.05
35	43.62 ± 0.33	0.1869 ± 0.0006	65.00 ± 0.05	21.65 ± 0.15	176.67 ± 0.75	299.21 ± 1.61
48	76.92 ± 0.58	0.1276 ± 0.0006	94.12 ± 1.35	30.61 ± 0.44	249.97 ± 2.93	420.41 ± 2.72
64	129.2 ± 1.0	0.1319 ± 0.0006	122.0 ± 0.4	40.69 ± 0.36	340.26 ± 2.68	581.36 ± 3.83
96	279.0 ± 2.6	0.1074 ± 0.0006	183.6 ± 1.5	65.51 ± 0.61	568.72 ± 2.92	986.67 ± 4.78
128	470.9 ± 4.7	0.0939 ± 0.0005	253.0 ± 4.9	86.69 ± 2.14	740.37 ± 8.36	1236.8 ± 6.0

Table 11. MC simulation data obtained for 3d Ising model with long-range correlated disorder: *averaging b*.

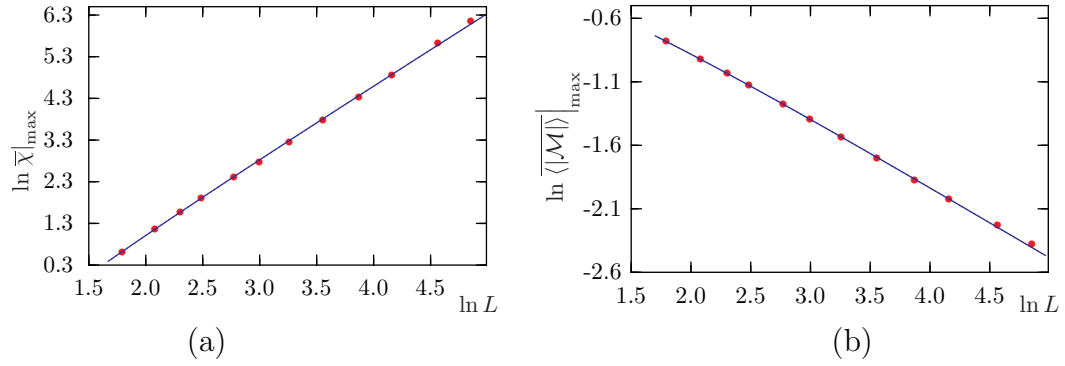


Figure 15. Log-log plots for the configurationally averaged maximum values of the magnetic susceptibility $\bar{\chi}_{\max}$ and magnetisation $\overline{\langle |\mathcal{M}| \rangle}_{\max}$. Solid line: data fit to the power law with the correction-to-scaling, Eq. (16).